Environmental Science & Technology

Article

pubs.acs.org/est

Formation of Pb(III) Intermediates in the Electrochemically Controlled Pb(II)/PbO_2 System

Haizhou Liu,*[,†] Andrey M. Kuznetsov,[‡] Alexey N. Masliy,[‡] John F. Ferguson,[§] and Gregory V. Korshin[§]

[†]Department of Civil and Environmental Engineering, University of California, Berkeley, California 94720, United States

[‡]Department of Inorganic Chemistry, Kazan National Research Technological University, K. Marx Street 68, Russian Federation 420015

[§]Department of Civil and Environmental Engineering, University of Washington, Box 352700, Seattle, Washington 98195-2700, United States

Supporting Information

ABSTRACT: The formation of lead dioxide PbO_2, an important corrosion product in drinking water distribution systems with lead-bearing plumbing materials, has been hypothesized to involve Pb(III) intermediates, but their nature and formation mechanisms remain unexplored. This study employed the electrochemical (EC) method of rotating ring disk electrode (RRDE) and quantum chemical (QC) simulations to examine the generation of intermediates produced during the oxidation of Pb(II) to PbO_2. RRDE data demonstrate that PbO_2 deposition and reduction involves at least two intermediates. One of them is a soluble Pb(III) species that undergoes further transformations to yield immobilized PbO_2 nanoparticles. The formation of this intermediate in EC system is mediated by hydroxyl radicals ($OH^•$), as was evidenced by the suppression of intermediates formation in the presence of the $OH^•$ scavenger *para*-chlorobenzoic acid. QC simulations confirmed that the oxidation of Pb(II) by $OH^•$ proceeds via Pb(III) species. These results show that Pb(III) intermediates play an important role in the reactions determining transitions between Pb(II) and Pb(IV) species and could impact lead release in drinking water.

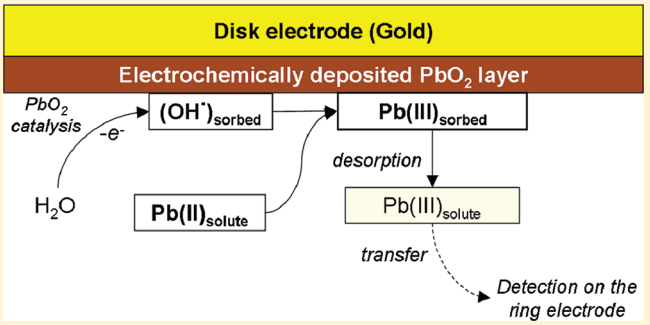

INTRODUCTION

Lead dioxide PbO_2 typically consisting of coalesced nanoparticles is commonly found on lead-containing plumbing materials exposed to drinking water containing chlorine.[1−3] Both scrutinyite α-PbO_2 and plattnerite β-PbO_2 form via the oxidation by chlorine of Pb(II) solids including hydrocerussite $Pb_3(CO_3)_2(OH)_2$, cerussite $PbCO_3$, and massicot PbO[1,4−6] or via the oxidation of Pb(II) solutes.[6] Because PbO_2 has a very low solubility, its presence is deemed to be beneficial for lead release control.

While free chlorine is still widely used for disinfection, many utilities have replaced chlorine with chloramines to reduce disinfection byproduct levels.[7] However, the switch of disinfectant has been associated with the destabilization of pre-existing PbO_2 and elevated lead in drinking water.[8,9] PbO_2 destabilization in the absence of chlorine proceeds via the reduction of PbO_2 to more soluble Pb(II) by natural organic matter,[10,11] products of chloramines decay,[12,13] and water per se,[12] as well as via colloidal mobilization of PbO_2 particles.[14,15]

Because of the complexity of Pb(II)/PbO_2 transformations and their implications to drinking water quality, it is important to understand mechanisms of reactions controlling the oxidation of Pb(II) to PbO_2 and the reduction of the latter. Prior investigations of PbO_2 formation have focused on the identification of batch oxidation products of Pb(II) precursors [1,6] or the analysis of structural composition of corrosion scales harvested from distribution systems.[2,3] These studies provided valuable information on maintaining the stability of PbO_2 but did not necessarily address the microscopic nature of Pb(II) to Pb(IV) transformations. Our prior studies showed that the oxidation by chlorine of typical Pb(II) solids such as hydrocerussite and cerussite is an autocatalytic reaction catalyzed by Pb(III) intermediates of largely unknown nature and/or nanosize nuclei of PbO_2.[4,5]

Pb(III) intermediates have only been observed in oxidations with γ-radiolysis, where Pb(II) hydroxo complex $Pb(OH)_3^-$ reacted with radiolytically generated hydroxyl radicals ($OH^•$) to produce short-lived Pb(III) species with a hypothetical stoichiometry of $Pb(OH)_4^-$ at pH higher than 11.[16] In addition, the presence of Pb(III) intermediates was only hypothesized during the deposition of crystalline PbO_2 in acidic media for battery applications.[17−20] However, these studies were carried out in chemical conditions too different from

Received: November 15, 2010
Revised: December 19, 2011
Accepted: December 22, 2011
Published: December 22, 2011

drinking water and did not examine the redox properties or molecular structures of Pb(III) intermediates.

Recent studies of the Pb(II)/PbO_2 redox system in conditions relevant to drinking water processes indicated a role of Pb(III) intermediates in the formation of surface phases of PbO_2. For instance, the reduction of PbO_2 to Pb(II) by bromide in acidic solution was hypothesized to proceed via two one-electron transfer steps with the formation of Pb(III) surface intermediates.[21] Examination of the oxidation of Pb(II) solids by chlorine [4,5,22] also suggested the formation of transient species prior to the generation of PbO_2 phase.

To systematically study the formation and redox properties of Pb(III) intermediates in the Pb(II)/PbO_2 system, an electrochemical (EC) technique of rotating ring disk electrode (RRDE) was applied to examine directly the generation of such intermediates during the EC formation and reduction of PbO_2. Quantum chemical (QC) simulations were performed to gain insight into the structures and ensuing transformations of Pb(III) species generated in these reactions.

MATERIALS AND METHODS

Electrochemical System. EC experiments were performed using a 125 mL three-electrode cell with a gold RRDE working electrode (Supporting Information Figure S1) affixed to a Pine AFMSRX rotator, a platinum counter electrode, and a Ag/AgCl reference electrode. The principles of intermediates detection is presented in the Supportin Information. The disk and ring electrodes were controlled by a Pine AFCBP1 bipotentiostat (Pine Instrument Co., Lawrence, KS). The outer diameters of the disk and ring electrodes were 4.57 mm and 5.38 mm, respectively. The ring−disk gap was 0.18 mm. For this electrode geometry and the electrolyte flow dynamics controlled by it, the highest theoretically predicted efficiency of collecting disk-electrode-generated mobile intermediates on the ring electrode is 28%.[23] The counter electrode was separated from the working electrode by a glass frit. EC potentials were measured and quoted vs the Ag/AgCl reference electrode (+0.197 V vs the standard hydrogen electrode, SHE).

Electrochemical and Morphological Measurements. All EC measurements were carried out in the presence of 0.1 M $NaClO_4$ background electrolyte at 22 ± 2 °C. Prior to each experiment, the surface of the RRDE was polished with microdiamond paste (particle size 0.25 μm) and rinsed with methanol and 0.01 M H_2SO_4 for 30 s, respectively, and finally with DI water. The reproducibility of the electrode surface preparation was confirmed by cyclic voltammetric (CV) scans in the background electrolyte. The concentration of Pb(II) in the solution was from 0.0001 to 0.005 M. pH values were fixed at 3, 4, or 5 by adding NaOH or $HClO_4$. Changes of pH during the CV experiments were within 0.1 units. In some experiments, 25 μM $OH^•$ radical scavenger *para*-chlorobenzoic acid (*p*CBA) was added to the Pb(II) solution. Before each experiment, solutions were purged with N_2 for 30 min to remove dissolved oxygen, and the EC cell was sealed with Teflon stoppers to prevent gas exchange with ambient air.

In CV measurements, the potential of the disk electrode (denoted as E_{disk}) was changed between −0.4 and 1.5 V at a constant scan rate ranging from 25 to 300 mV/s, while the potential of the ring electrode (referred to as E_{ring}) was kept constant between 0.5 and 1.3 V. EC currents corresponding to the redox reactions at both electrodes were recorded.

To examine the structure of PbO_2 deposited on the electrode, a 4-cm gold wire with a diameter of 0.025 cm (Sigma-Aldrich Inc.) was alternatively used as the working electrode. Sections of the gold wire were removed from the cell after EC experiments and air-dried. The morphology of PbO_2 phases was analyzed with a JEOL JSM-7400F Scanning Electron Microscope (SEM) (JEOL Ltd., Tokyo, Japan).

Quantum Chemical Calculations. QC modeling was carried out using the Gaussian 09 program package to examine the structure and thermodynamic properties of Pb(III) intermediates. The simulation was based on the density functional theory with ωB97X functional that accounts for long-range corrections and generates more accurate results on kinetic and structural properties of noncovalent interactions.[24−26] Atomic orbitals of O and H atoms were described using the electron correlated aug-cc-pvdz basis set.[24,27] For Pb atoms, a small-core electron effective pseudopotential (ECP) with the aug-cc-pvdz-PP basis set was used.[28] All computations were performed with the full optimization of molecular geometry without any symmetry constrains taking into account solvent effects. This optimization was followed by calculations of vibrational spectra to ensure that the optimized geometries correspond to minima on the total potential energy surfaces (no imaginary frequencies). These calculations were also used to evaluate the thermal and vibrational corrections to the enthalpies and the Gibbs free energies (at 298 K and 1 Atm). Solvent effects were accounted for using the integral equation formalism version (IEFPCM) of the polarizable continuum model (PCM).[29] Graphical processing of QC data was carried out with ChemCraft software.[30]

RESULTS AND DISCUSSION

Features of Electrochemical Oxidation of Pb(II). CV scans obtained from the Pb(II)/RRDE system had prominent features that depended on scan rate, rotation speed, solution pH, and evolution of the electrode surface. In static electrode conditions, the first anodic scan carried with E_{disk} potential from −0.4 to 1.5 V showed only one peak with the maximum at approximately 1.2 V (Figure 1A). This peak is denoted henceforth as Peak 2.

The EC potential corresponding to the Pb(II)/PbO_2 couple can be calculated based on the following expression:

$$Pb^{2+} + 2H_2O - 2e^- \rightarrow PbO_2 + 4H^+ \qquad E^0 = 1.46\ V \qquad (1)$$

Under the conditions shown in Figure 1, the EC potential of reaction 1 is 1.1 V vs the Ag/AgCl electrode (Supporting Information Figure S2). The fact that Peak 2 emerged at potentials higher than this threshold indicated that this peak was associated with the EC oxidation of Pb(II) to PbO_2. Sequential EC oxidations following the first cycle were accompanied by the emergence of another peak denoted as Peak 1 (Figure 1A). Because Peak 1 emerged at E_{disk} potentials much lower than those of Peak 2 (0.7 to 0.9 V), it corresponded to a reaction involving the oxidation of Pb(II) to intermediate products.

Repeated experiments carried out at E_{disk} less than 1.1 V did not result in PbO_2 formation or the occurrence of Peak 1 (Supporting Information Figure S3). SEM examination confirmed that only EC scans exceeding E_{disk} of 1.1 V were accompanied by the formation of a PbO_2 phase which also modified the electrode surface (Figure 2). After the first scan, isolated PbO_2 nanoparticles with sizes around 30 nm were deposited on the surface (Figure 2A). As the scans continued,

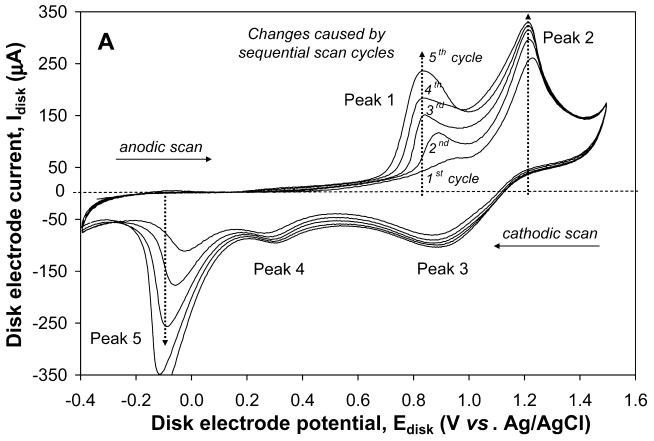

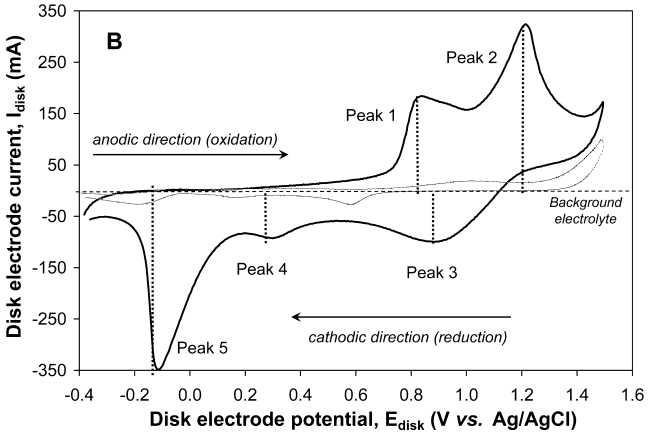

Figure 1. Main features of voltammetric scans for static gold disk electrode in 0.003 M $Pb(ClO_4)_2$ solution, pH 5.0, scan rate 75 mV/s. (A) Effects of sequential scans on the evolution of Peaks 1 and 2; (B) positions of main peaks.

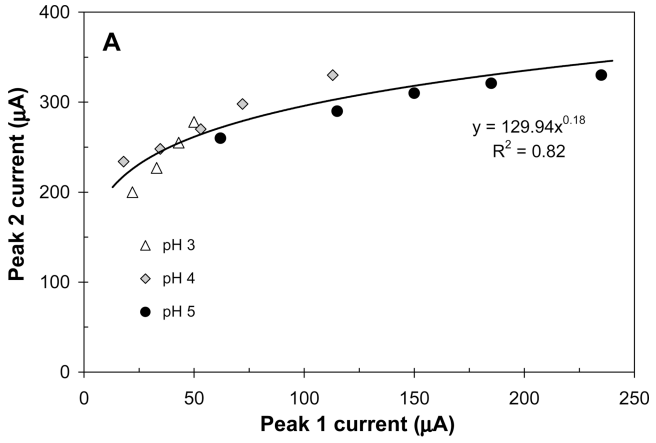

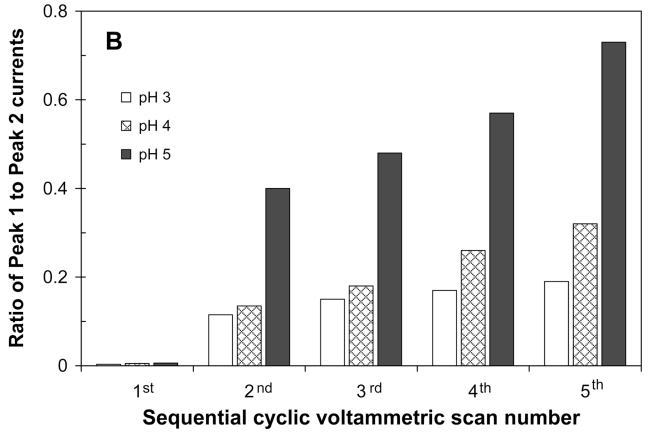

Figure 3. Impact of pH on the EC oxidation of Pb(II) and intermediates formation. Scan rate 75 mV/s, 0.003 M $Pb(ClO_4)_2$, static electrode. (A) Correlation between intensities of Peak 1 and Peak 2; (B) effects of pH on ratios of Peak 1 and Peak 2 currents.

more PbO_2 was accumulated on the electrode and the deposited PbO_2 nuclei aggregated into larger clusters with sizes of approximately 100 nm (Figure 2B). Morphologically, they were indistinguishable from PbO_2 crystallites formed during the oxidation of cerussite and hydrocerussite by chlorine.[1,4−6]

Peak 1 gained more intensity after each sequential scan and was more sensitive to the solution pH than Peak 2 (Figure 3A). The ratio of intensities of Peak 1 to Peak 2 increased prominently as a result of the number of scan cycles and also with the increase of solution pH (Figure 3B). The effect of pH indicates that Pb(II) hydroxo complexes were more reactive than free Pb(II) ions in reactions associated with Peak 1, and adsorbed OH^- ions may contribute to that reaction. It was also observed that the intensities of Peaks 1 and 2 increased by 2−3 times in rotating electrode conditions (Supporting Information

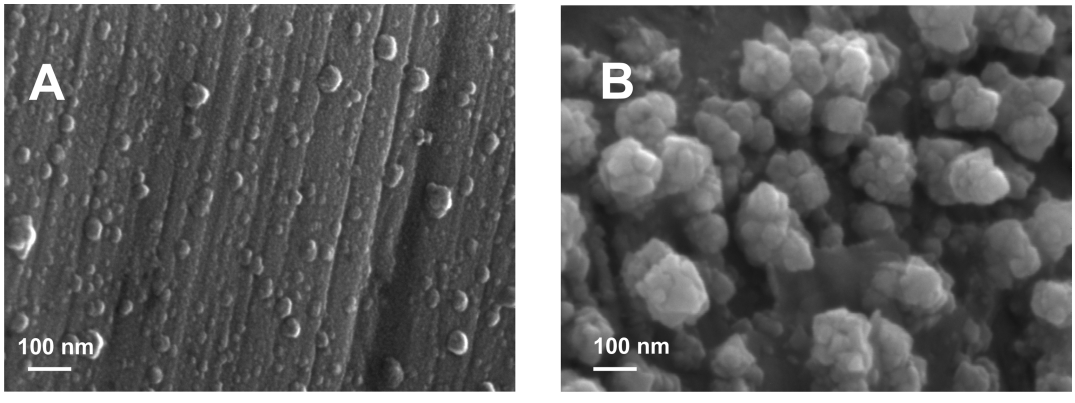

Figure 2. Formation of PbO_2 from Pb(II) on the gold electrode surface during sequential cyclic voltammetric scans between −0.4 and 1.5 V. 0.003 M $Pb(ClO_4)_2$, pH 4.0, background electrolyte 0.1 M $NaClO_4$, scan rate 50 mV/s. (A) after 1st scan cycle: incipient formation of PbO_2 nanophase; (B) after 5th scan cycle: formation of large PbO_2 clusters.

dx.doi.org/10.1021/es203084n | Environ. Sci. Technol. 2012, 46, 1430−1438

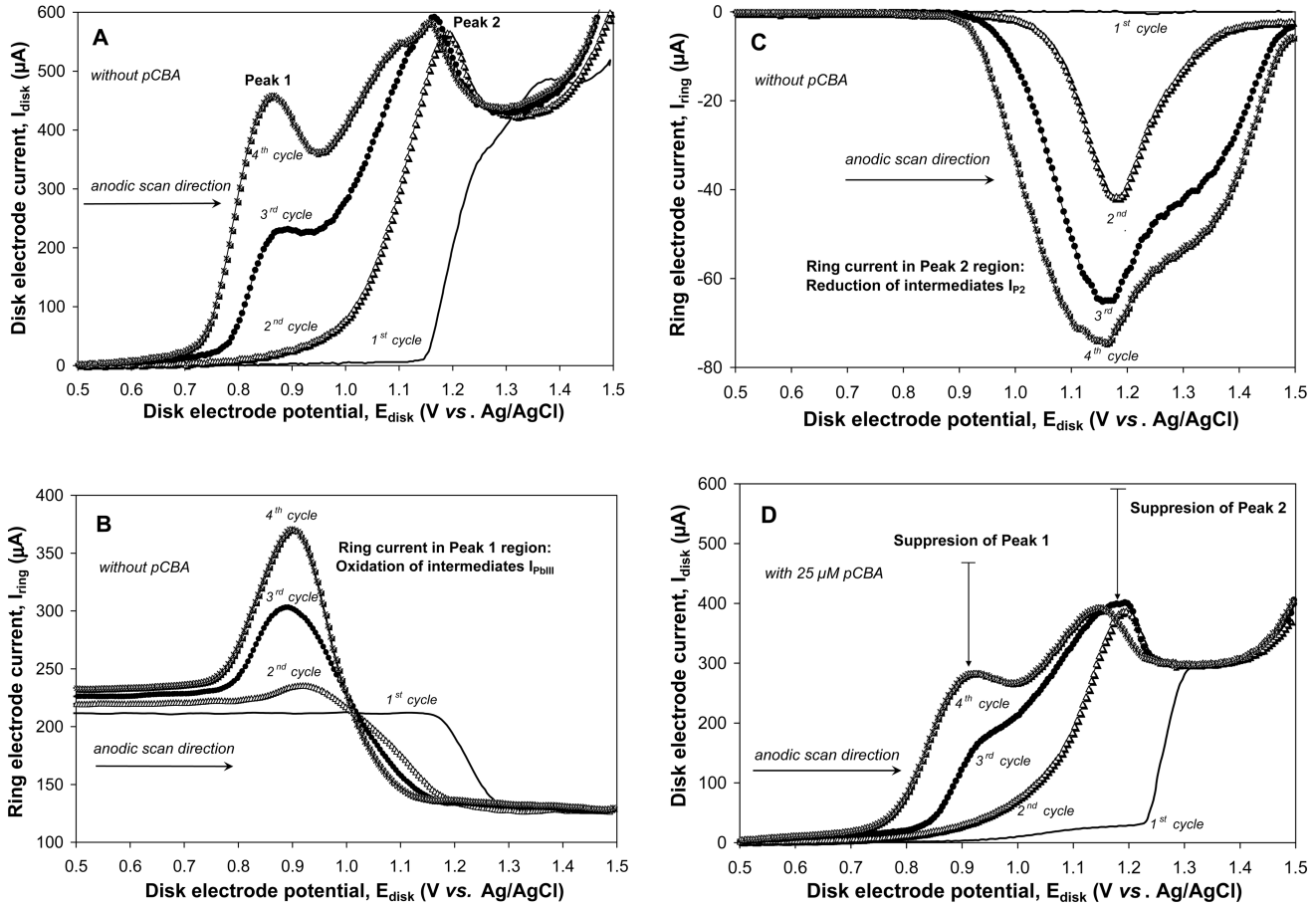

Figure 4. Detection of intermediates from ring currents for EC oxidation of 0.003 M $Pb(ClO_4)_2$. Gold rotating ring disk electrode, rotation speed 500 rpm, scan rate 50 mV/s. Background electrolyte 0.1 M $NaClO_4$, pH 4.0. (A) Disk current; (B) ring current at a fixed ring potential of 1.3 V; (C) ring current at a fixed ring potential of 0.7 V; (D) disk current with 25 μM *p*CBA.

Figure S4), suggesting Pb(II) diffusion from bulk solution to the electrode limited the overall reaction rate.

Three peaks corresponding to the cathodic reduction of PbO_2 on the disk electrode were observed. The maxima of these peaks (denoted as Peaks 3, 4, and 5) were located at approximately 0.9, 0.3, and −0.1 V, respectively (Figure 1B). The intensities of Peaks 3 and 4 were not appreciably sensitive to the number of sequential scan cycles, but the intensity of Peak 5 increased steadily in these conditions (Figure 1A). In rotating electrode conditions, Peaks 3 and 4 totally disappeared while the intensity of Peak 5 underwent a nearly threefold increase (Supporting Information Figure S4). These observations indicated that Peaks 3 and 4 were associated with the reduction of hydrodynamically mobile Pb(IV) species, likely precursors of PbO_2 nanoparticles. In contrast, Peak 5 corresponds to the reduction of PbO_2 particles deposited on the electrode surface. Because the amount of PbO_2 deposited on the disk electrode increased after each voltammetric scan and the convection of Pb(II) to the electrode surface was enhanced by rotation, the intensity of Peak 5 increased accordingly.

EC-Generation of Intermediates during PbO_2 Formation and Reduction. The presence of intermediates formed upon the EC oxidation of Pb(II) was confirmed by the ring electrode data obtained in rotating conditions (Figure 4). At pH 4.0 and a scan rate of 50 mV/s, Peak 1 and Peak 2 occurred on the disk electrode similarly to static conditions, and their intensities increased with the number of cycles (Figure 4A).

When the ring electrode potential (denoted as E_{ring}) was set at 1.3 V, the ring current was constant during the first anodic cycle except decreasing at E_{disk} over 1.2 V (Figure 4B). At E_{disk} over 1.2 V, the amount of Pb(II) transferred by convection from the disk to the ring decreased due to the oxidation of Pb(II) at the disk electrode. However, following the initial deposition of PbO_2 nuclei on the disk after the first scan cycle, the ring current increased notably at E_{disk} potentials located in the Peak 1 region (Figure 4B). Each subsequent cycle that deposited an additional PbO_2 on the disk was accompanied by additional increases of the ring current. This indicated that a hydrodynamically mobile intermediate (denoted henceforth as I_{PbIII}) was formed during the oxidation of Pb(II) on the disk electrode and further oxidized on the ring electrode.

Examination of ring currents observed in the E_{disk} range close to Peak 2 (from 1.0 to 1.4 V) showed that another EC-active species was generated only after the first anodic scan. In contrast with intermediate I_{PbIII}, the latter species underwent reduction at the ring when the E_{ring} value was set at 0.7 V (Figure 4C). This intermediate (denoted as I_{P2}) was formed at the disk in Peak 2 region. The reduction of intermediate I_{P2} on the ring was observed in the range of E_{ring} from 0.6 to 0.8 V with a maximum at 0.7 V (Supporting Information Figure S5). The reduction of PbO_2 deposited on the disk and manifesting itself as Peak 5 was also accompanied by the generation of an

dx.doi.org/10.1021/es203084n | Environ. Sci. Technol. 2012, 46, 1430−1438

EC-active intermediate whose oxidation also took place in the range of E_{ring} values 0.6 to 0.8 V (Supporting Information Figure S6). This intermediate was denoted as I_{P3}.

Because PbO_2 was not formed prior to the first anodic scan, the fact that ring currents occurred and increased only after the first scan cycle suggested that the intermediates originated from a reaction that occurred only in the presence of EC-deposited PbO_2 and was catalyzed by it. Prior studies show that anodically polarized PbO_2 is characterized by high yield of $OH^•$ radicals.[31,32] During anodic scans, $OH^•$ radicals can be produced on the disk electrode that is deposited with PbO_2 and interact with Pb(II) to yield Pb(III) intermediates.

To examine the hypothesis that $OH^•$ radicals generated on the disk electrode are implicated in the generation of intermediate I_{PbIII}, EC experiments were carried out in the presence of *p*CBA that reacts readily with $OH^•$ radicals.[33,34] *p*CBA does not interfere with the electrode surface or Pb species,[32] and its presence did not cause any appreciable changes of the disk currents in the background CV scans. Therefore, *p*CBA acted exclusively as a $OH^•$ radical scavenger in the EC system. It was found that the presence of 25 μM *p*CBA suppressed Pb(II) oxidation currents and resulted in less prominent peaks. For instance, the intensity of Peak 1 after four scan cycles was reduced by 40% (Figure 4D) compared with that in the absence of *p*CBA (Figure 4A). Additionally, ring currents for Peak 2 were suppressed in the presence of *p*CBA (Supporting Information Figure S7). These results support the notion that intermediate I_{PbIII} is formed via the oxidation of Pb(II) ions by $OH^•$ radicals produced at the surface of the EC-deposited PbO_2.

Examination of relationships between Peak 1 and Peak 5 currents exhibited a strong linear correlation that passed through the origin of the coordinates (Figure 5A). Because Peak 1 and Peak 5 correspond to the production of mobile intermediate I_{PbIII} and the reduction of EC-deposited PbO_2 nanoparticles, respectively, the concerted behavior of these two peaks suggested that the generation of Pb intermediates is intrinsically associated with the formation of PbO_2 from oxidizing Pb(II).

In contrast, correlation between Peak 2 and Peak 5 currents never passed through the origin of the coordinates (Figure 5B). Peak 2 was present in the voltammetric scans irrespective of the presence of PbO_2. Because EC reactions in the Peak 2 region were still necessary to initiate the deposition of PbO_2, only a small fraction of EC reactions at Peak 2 potentials was associated with further oxidation of intermediate I_{PbIII} (formed at Peak 1 potentials) to PbO_2. The remainder of EC currents in the Peak 2 region is likely to be associated with the formation of the other intermediate I_{P2} that did not contribute to the generation of PbO_2 solid.

Quantum Chemical Simulations of Pb(II) and Pb(III) Reactions. To gain deep insight into the nature of intermediate I_{PbIII}, QC modeling of Pb(II) and Pb(III) reactions was carried out. It started with the examination of the structure of the Pb(II) aqua-complex. Recent experiments show that it tends to have six water molecules in the inner shell, and they cluster on one side of the central Pb^{2+} ion to form an asymmetric (hemi-directed) structure as opposed to a symmetric (holo-directed) distribution of the inner shell water molecules.[35−37] Optimization of the geometry of Pb(II) aqua-complex $Pb(H_2O)_6^{2+}$ showed the presence of a pronouncedly hemi-directed arrangement of water molecules (Supporting Information Figure S8-A) in accord with prior

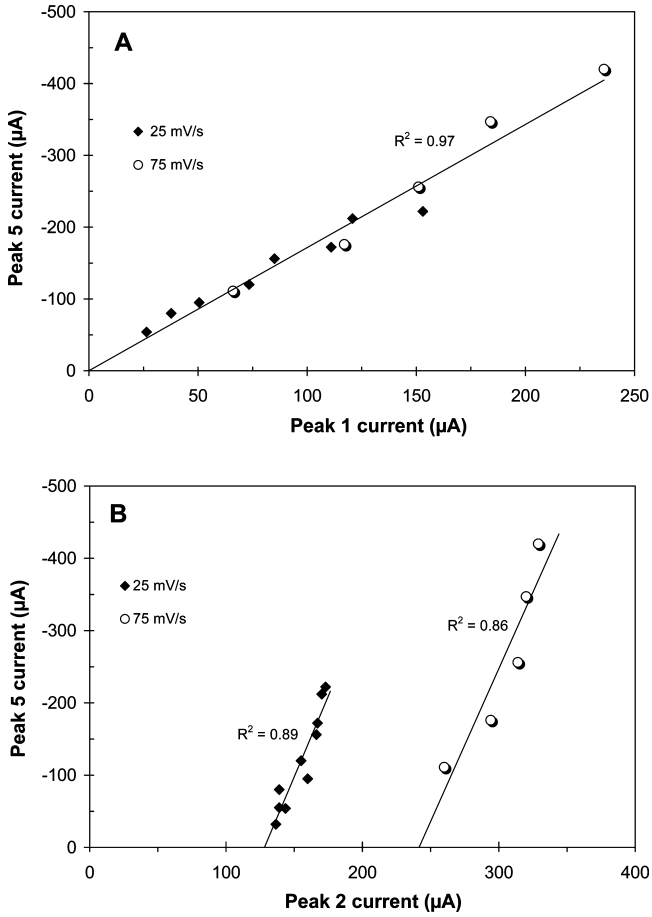

Figure 5. (A) Correlation between intensities of Peak 5 and Peak 1 and (B) correlation between intensities of Peak 5 and Peak 2. Data for CV scans in 0.003 M solutions of $Pb(ClO_4)_2$, pH 4 and 5, varying scan rates.

experimental data.[37] The average Pb−O distance determined for the $Pb(H_2O)_6^{2+}$ ion is 2.59 Å, which compares well with the experimental observations of 2.54 Å.[37] Further simulations of Pb(II) hydroxo complexes predicted that the presence of OH^- ions in the inner shell of Pb(II) caused the water molecules to migrate to the second hydration shell where they formed hydrogen bonds with the inner sphere ligands. The resultant stoichiometries of thermodynamically favored Pb(II) hydroxo complexes were determined as $Pb(OH)(H_2O)_4^+$, $Pb(OH)_2(H_2O)_2$, $Pb(OH)_3^-$, and $Pb(OH)_4^{2-}$ (Figure 6A−D).

Interaction of $OH^•$ radical with $Pb(H_2O)_6^{2+}$ was simulated by adding an $OH^•$ radical to the $Pb(H_2O)_6^{2+}$ ion to form a $Pb(OH)(H_2O)_6^{•2+}$ complex with an initial Pb···$OH^•$ separation of about 3 Å. This configuration was optimized to yield the structure shown in Supporting Information Figure S8-B. The entry of $OH^•$ into the inner shell resulted in a negligible effective positive charge on the $OH^•$. This particle interacted with the central Pb ion via a weak ion-dipole electrostatic mechanism that resulted in a small negative enthalpy (ΔH^0) value (reaction 1,Table 1). Attempts to force the $OH^•$ radical to approach the central Pb^{2+} ion to a 2.2 to 2.4 Å distance characteristic for Pb(II) hydroxo complexes (Figure 6A−D) resulted in, after full optimization of this starting geometry, the withdrawal of the introduced $OH^•$ radical back to the initial structure shown in Supporting Information Figure S8-A. The effective positive charge on the central Pb ion (+1.8) did not

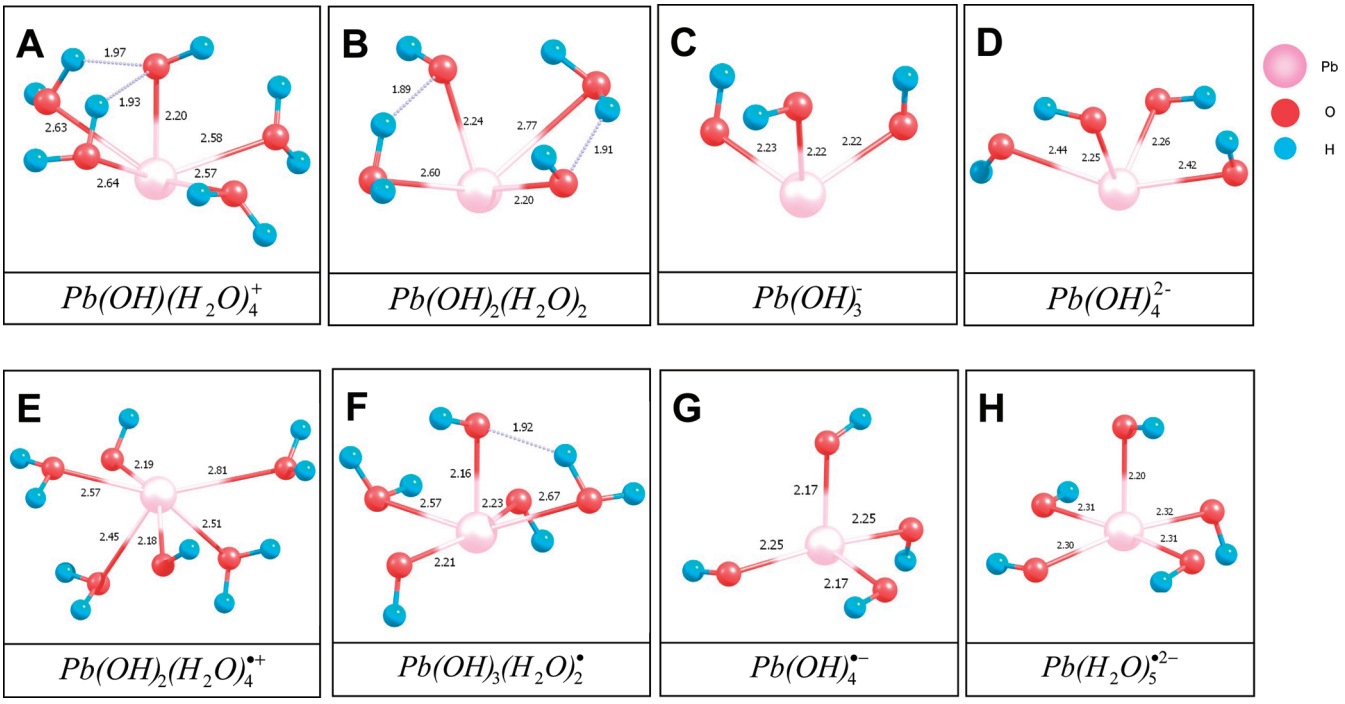

Figure 6. (A–D) Optimized structures of Pb(II) hydroxo complexes and (E–H) structures of the corresponding Pb(III) intermediates formed as a result of the oxidation of Pb(II) hydroxo complexes by $OH^{\bullet}$ radical (reactions 2–5, Table 1).

Table 1. Thermodynamic Quantum Chemical Data for Reactions of Pb(II) and Pb(III) Species

Reaction	Enthalpy ΔH^0 (kcal/mol)	Entropy ΔS^0 (cal/mol·K)	Energy ΔG^0 (kcal/mol)
Non-oxidative addition of hydroxyl radical to Pb(II) aqua-complexes			
1. $Pb^{II}(H_2O)_6^{2+} + OH^{\bullet} \rightarrow Pb^{II}(OH)(H_2O)_6^{\bullet 2+}$	-4.43	-32.9	5.38
Oxidation of Pb(II) complexes by hydroxyl radical to form Pb(III) intermediates			
2. $Pb^{II}OH(H_2O)_4^{+} + OH^{\bullet} \rightarrow Pb^{III}(OH)_2(H_2O)_4^{\bullet +}$	-6.46	-24.7	0.90
3. $Pb^{II}(OH)_2(H_2O)_2 + OH^{\bullet} \rightarrow Pb^{III}(OH)_3(H_2O)_2^{\bullet}$	-11.42	-25.0	-3.97
4. $Pb^{II}(OH)_3^{-} + OH^{\bullet} \rightarrow Pb^{III}(OH)_4^{\bullet -}$	-19.46	-30.2	-10.46
5. $Pb^{II}(OH)_4^{2-} + OH^{\bullet} \rightarrow Pb^{III}(OH)_5^{\bullet 2-}$	-27.46	-26.7	-19.79
Oxidation of Pb(III) intermediates by hydroxyl radical			
6. $Pb^{III}(OH)_2(H_2O)_4^{\bullet +} + OH^{\bullet} \rightarrow Pb^{IV}(OH)_3(H_2O)_3^{+} + H_2O$	-48.20	-56.4	-31.40
7. $Pb^{III}(OH)_3(H_2O)_2^{\bullet} + OH^{\bullet} \rightarrow Pb^{IV}(OH)_4(H_2O)_2$	-48.42	-36.5	-37.53
8. $Pb^{III}(OH)_4^{\bullet -} + OH^{\bullet} \rightarrow Pb^{IV}(OH)_5^{-}$	-55.45	-37.4	-44.31
9. $Pb^{III}(OH)_5^{\bullet 2-} + OH^{\bullet} \rightarrow Pb^{IV}(OH)_6^{2-}$	-65.59	-43.3	-52.68
Dimerization and Disproportionation of Pb(III) intermediates			
10. $2Pb^{III}(OH)_2(H_2O)_4^{\bullet +} \rightarrow Pb^{II}OH(H_2O)_4^{+} + Pb^{IV}(OH)_3(H_2O)_3^{+} + H_2O$	-41.70	-31.7	-32.30
11. $2Pb^{III}(OH)_3(H_2O)_2^{\bullet} \rightarrow Pb^{II}(OH)_2(H_2O)_2 + Pb^{IV}(OH)_4 + 2H_2O$	-29.61	56.7	-43.81
12. $Pb^{III}(OH)_4^{\bullet -} + Pb^{III}(OH)_2(H_2O)_4^{+} \rightarrow Pb^{II}(OH)_2(H_2O)_2 + Pb^{IV}(OH)_4 + 2H_2O$	-24.72	49.4	-49.54
13. $2Pb^{III}(OH)_4^{\bullet -} \rightarrow Pb^{II}(OH)_4^{2-} + Pb^{IV}(OH)_4$	-0.67	1.9	-1.24
14. $2Pb^{III}(OH)_2(H_2O)_4^{\bullet +} \rightarrow Pb^{II}(H_2O)_6^{2+} + Pb^{IV}(OH)_4 + 2H_2O$	-43.44	-10.4	40.35
15. $2Pb^{III}(OH)_2(H_2O)_4^{\bullet +} \rightarrow Pb^{II}(OH)_2(H_2O)_2 + Pb^{IV}(OH)_2(H_2O)_2^{2+} + 4H_2O$	40.59	94.2	12.50

change appreciably when going from $Pb(H_2O)_6^{2+}$ to $Pb(OH)(H_2O)_6^{\bullet 2+}$, indicating that the addition of an $OH^{\bullet}$ radical to $Pb(H_2O)_6^{2+}$ has a nonoxidative character.

Simulations of interactions of $OH^{\bullet}$ radicals with Pb(II) hydroxo complexes showed a different trend. The Gibbs free energy (ΔG^0) corresponding to the entry of an $OH^{\bullet}$ radical into the inner shell of these complexes decreases with the number of hydroxo groups, indicating increasing thermodynamic likelihood of these reactions (reactions 2–5, Table 1). This is consistent with the EC data demonstrating a pronouncedly more rapid onset of the generation of Pb(III)

dx.doi.org/10.1021/es203084n | Environ. Sci. Technol. 2012, 46, 1430–1438

intermediates and their higher yields at increasing pHs (Figure 3).

QC simulations showed that the $OH^{\bullet}$ radical entering the inner shell of Pb(II) hydroxo complexes acquires a substantial negative charge and becomes nearly identical to the hydroxo groups initially present in the structure. At the same time, the central Pb atom becomes essentially a radical because the major part of the uncoupled electron's density is located on it. The Pb−OH distances in $Pb(OH)_2(H_2O)_4^{\bullet+}$, $Pb(OH)_3(H_2O)_2^{\bullet}$, $Pb(OH)_4^{\bullet-}$, and $Pb(H_2O)_5^{\bullet 2-}$ formed via the interactions of $OH^{\bullet}$ with Pb(II) hydroxo complexes ranging from 2.16 to 2.32 Å (Figure 6E−H), much shorter than that in $Pb(OH)(H_2O)_6^{\bullet 2+}$ (2.69 Å). The effective positive charges on the central Pb atom in these intermediates formed by $OH^{\bullet}$ radical (Figure 6E−H) are approximately 0.3 to 0.4 more positive compared to those in initial Pb(II) complexes (Figure 6A−D). This indicates that the entry of an $OH^{\bullet}$ radical into the inner shell of the Pb(II) hydroxo complexes is a reaction of oxidative addition, and the central Pb atoms can be formally assigned a +3 oxidation state.

The thermodynamics of reactions of Pb(III) species showed that they are susceptible to further oxidation to yield Pb(IV) complexes that can be considered as precursors of PbO_2. ΔG^0 values corresponding to the oxidation of $Pb(OH)_2(H_2O)_4^{\bullet+}$and $Pb(OH)_3(H_2O)_2^{\bullet}$ by $OH^{\bullet}$ radicals are −31.4 and −37.5 kcal/mol, respectively (reactions 6 and 7, Table 1). The oxidation of $Pb(OH)_4^{\bullet-}$ and $Pb(H_2O)_5^{\bullet 2-}$ are expected to predominate at high pHs have ΔG^0 values of −44.3 and −52.7 kcal/mol, respectively (reactions 8 and 9, Table 1).

QC calculations also demonstrated that, in accord with the data of radiolysis experiments,[16,20] Pb(III) intermediates can undergo dimerization/disproportionation to yield Pb(II) and Pb(IV) species (reactions 10−15, Table 1). ΔG^0 values corresponding to some of these reactions (reactions 10 and 11, Table 1) are slightly lower than those determined for the oxidation of Pb(III) intermediate by $OH^{\bullet}$ radical (reactions 6 and 7, Table 1). Pb(IV) complexes (reactions 10−12 and 14, Table 1) are expected to undergo further transformations to form solid PbO_2 phase.[4,5,16,17,19]

Synthesis of EC and QC Data on Pb(III) Formation. EC data demonstrate that traces of PbO_2 nanoparticles deposited on the electrode after the first CV cycle initiate and catalyze the EC generation of $OH^{\bullet}$ radicals, which by reacting preferentially with Pb(II) hydroxo complexes produce Pb(III) intermediates associated with Peak 1. While concentrations of Pb(II) hydroxo complexes are low at pH less than 5, the possibility that they have a much higher reactivity in EC oxidations was confirmed by QC simulations that determine that these intermediates are likely to be $Pb(OH)_2(H_2O)_4^{\bullet+}$ and $Pb(OH)_3(H_2O)_2^{\bullet}$ (reactions 2 and 3, Table 1).

These Pb(III) species can be directly EC-oxidized or interact with EC-generated $OH^{\bullet}$ radicals to form PbO_2 precursors. These reactions are associated with Peak 2 in the EC system. Their occurrence is also supported by the QC predictions (reactions 6 and 7, Table 1). Alternatively, when the concentration of Pb(III) species at the surface is high enough, they are likely to dimerize and disproportionate to yield Pb(IV) species, for example, $Pb(OH)_3(H_2O)_3^{+}$ and $Pb(OH)_4^{0}$, (reactions 10 and 14, Table 1) and undergo further transformations to form PbO_2.

Environmental Implications. The electrochemical technique used in this study allowed for in situ detection of Pb(III) intermediates generated during the EC oxidation of Pb(II). Quantum chemical simulations examined the microstructure and thermodynamic properties of Pb(III) species in solution chemistry with $OH^{\bullet}$ radicals. Despite that reactions in the distribution system involve surfaces of lead oxide particles, simulation data unambiguously characterized the reaction pathways involving Pb(III).

Although redox controls in drinking water distribution systems with lead-containing plumbing materials and residual chlorine may be different from those in the studied EC-controlled system because in the latter case the formation of Pb(III) is driven by EC-generated $OH^{\bullet}$ radicals while in water distribution systems Pb(II) oxidation is driven by the $HOCl/Cl^{-}$ couple, the intrinsic aspects of the redox chemistry of the Pb(II)/Pb(IV) couple are fundamentally the same in both cases. Thus, the reported measurements of Pb(III) by means of analytical electrochemistry prove that Pb(III) intermediates and Pb(III) generation mechanisms are likely to play an important role in Pb(II) oxidation processes in drinking water conditions. The reduction and destabilization of PbO_2 also involve transient species.

Prior research in environmental systems reported the catalytic role of PbO_2 in the oxidation by chlorine of Pb(II) hydroxylcarbonates,[4] the occurrence of distinct attack sites on the surfaces of these solids which are indicative of the generation of soluble intermediates,[5] and the hypothesized formation of a Pb(III) surface complex during the reduction of PbO_2 by Br^{-},[21] which all agree with this study concerning the formation of Pb intermediates during Pb(II)/Pb(IV) redox transformations. In drinking water distribution systems, the generation of Pb(III) from Pb(II) can be at least partially driven by the formation of $Cl^{\bullet}$ radical from HOCl as a one-electron transfer step, catalyzed by PbO_2 in the corrosion scales.[4] Data from prior studies have suggested that the $Cl^{\bullet}$ radical reacts with water to generate the $OH^{\bullet}$ radical.[38−40] An estimation based on the reported kinetics data [4,5,38−40] indicates that the steady-state concentration of the $OH^{\bullet}$ radical in these conditions may be on the order of 10^{-12} M.

Water chemistry can strongly influence the formation of Pb(III) intermediates in a distribution system. Our EC data demonstrate that higher pHs favor the formation of one type of Pb(III) intermediates whose presence eventually leads to the deposition of immobilized PbO_2 nanoparticles, while the formation of the other intermediate that results in mobile Pb(IV) precursors is not very sensitive to pH. Quantum chemical simulations show that this is related to the higher reactivity of Pb(II) hydroxo complexes. However, the concentration of HOCl decreases fast at pH higher than 7 and OCl^{-} is largely unreactive toward Pb(II) species (pK_{HOCl} = 7.6). Therefore, there is likely a range of optimal pHs that benefit from the formation of a stable PbO_2 phase in chlorinated water.

Increase of alkalinity in drinking water will increase the concentration of Pb(II) carbonate complexes. Although we did not examine their effects in the EC system, prior research has demonstrated that Pb(II) carbonate complexes are much less reactive with chlorine than Pb(II) hydroxo complexes.[4−6] Accordingly, the formation of Pb(III) intermediates is expected to be slower in high alkalinity water. Natural organic matter (NOM) in drinking water can form complexes with Pb(II) and possibly Pb(III) species and also scavenge $Cl^{\bullet}$ and $OH^{\bullet}$ radicals, thus ultimately affecting the yields of the intermediates. The identities and actual occurrence formed in the presence of NOM will be elucidated in the future.

■ ASSOCIATED CONTENT

Supporting Information

Eight figures show the configuration and working principles of the EC experimental system, additional SEM and CV data for EC oxidations of Pb(II) in static and rotating conditions, and selected QC data. This material is available free of charge via the Internet at http://pubs.acs.org.

■ AUTHOR INFORMATION

Corresponding Author

*E-mail: haizhou@berkeley.edu. Phone: (510) 643-0355.

■ ACKNOWLEDGMENTS

This study was supported by U.S. National Science Foundation (#0504447 and partially #0931676). We thank Archana Kasinathan for participating in experimental activities. H.L. also thanks the Electrochemical Society for their research fellowship.

■ REFERENCES

(1) Lytle, D. A.; Schock, M. R. Formation of Pb(IV) oxides in chlorinated water. *J. Am. Water Works Assoc.* **2005**, *97* (11), 102−114.

(2) Edwards, M.; Dudi, A. Role of chlorine and chloramine in corrosion of lead-bearing materials. *J. Am. Water Works Assoc.* **2004**, *96* (10), 69−81.

(3) Kim, E. J.; Herrera, J. E. Characteristics of lead corrosion scales formed during drinking water distribution and their potential influence on the release of lead and other contaminants. *Environ. Sci. Technol.* **2010**, *44* (16), 6054−6061.

(4) Liu, H.; Korshin, G. V.; Ferguson, J. F. Investigation of the kinetics and mechanisms of the oxidation of cerussite and hydrocerussite by chlorine. *Environ. Sci. Technol.* **2008**, *42* (9), 3241−3247.

(5) Liu, H.; Korshin, G. V.; Ferguson, J. F. Interactions of Pb(II)/Pb(IV) solid phases with chlorine and their effects on lead release. *Environ. Sci. Technol.* **2009**, *43* (9), 3278−3284.

(6) Wang, Y.; Xie, Y.; Li, W.; Wang, Z.; Giammar, D. E. Formation of lead(IV) oxides from lead(II) compounds. *Environ. Sci. Technol.* **2010**, *44* (23), 8950−8956.

(7) Seidel, C. J.; McGuire, M. J.; Summers, S.; Via, S. Have utilities switched to chloramines? *J. Am. Water Works Assoc.* **2005**, *97* (10), 87−97.

(8) Rajasekharan, V. V.; Clark, B. N.; Switzer, J. A. Electrochemistry of free chlorine and monochloramine and its relevance to the presence of Pb in drinking water. *Environ. Sci. Technol.* **2007**, *41* (12), 4252−4257.

(9) Brown, M. J.; Raymond, J.; Homa, D.; Kennedy, C.; Sinks, T. Association between children's blood levels, lead service lines, and water disinfection, Washington, DC, 1998−2006. *Environ. Res.* **2011**, *111* (1), 67−74.

(10) Lin, Y. P.; Valentine, R. L. The release of lead from reduction of lead oxide (PbO_2) by natural organic matter. *Environ. Sci. Technol.* **2008**, *42* (3), 760−765.

(11) Dryer, D. J.; Korshin, G. V. Investigation of the reduction of lead dioxide by natural organic matter. *Environ. Sci. Technol.* **2007**, *41* (15), 5510−5514.

(12) Lin, Y. P.; Valentine, R. L. Release of Pb(II) from monochloramine-mediated reduction of lead oxide (PbO_2). *Environ. Sci. Technol.* **2008**, *42* (24), 9137−9143.

(13) Lin, Y. P.; Valentine, R. L. Reduction of lead oxide (PbO_2) and release of Pb(II) in mixtures of natural organic matter, free chlorine and monochloramine. *Environ. Sci. Technol.* **2009**, *43* (10), 3872−3877.

(14) Xie, Y.; Wang, Y.; Singhal, V.; Giammar, D. E. Effects of pH and carbonate concentration on dissolution rates of the lead corrosion product PbO_2. *Environ. Sci. Technol.* **2010**, *44* (3), 1093−1099.

(15) Triantafyllidou, S.; Parks, J.; Edwards, M. Lead particles in potable water. *J. Am. Water Works Assoc.* **2007**, *99* (6), 107−117.

(16) Mosseri, S.; Henglein, A.; Janata, E. Trivalent lead as an intermediate in the oxidation of Pb^{II} and the reduction of Pb^{IV} species. *J. Phys. Chem.* **1990**, *94* (6), 2722−2726.

(17) Velichenko, A. B.; Girenko, D. V.; Danilov, F. I. Electrodeposition of lead dioxide at an Au electrode. *Electrochim. Acta* **1995**, *40* (17), 2803−2807.

(18) Hampson, N. A. The aqueous system Pb^{4+}/Pb^{2+}: Electrochemical Aspect. *The electrochemistry of lead*; Academic Press: London, 1979.

(19) Velichenko, A. B.; Girenko, D. V.; Danilov, F. I. Mechanism of lead dioxide electrodeposition. *J. Electroanal. Chem.* **1996**, *405* (1), 127−132.

(20) Gogolev, A. V.; Makarov, I. E.; Pikaev, A. K. Pulse radiolysis of aqueous hydrochloric solutions of lead ions. *High Energy Chem.* **1984**, *18*, 336−339.

(21) Lin, Y. P.; Valentine, R. L. Reductive dissolution of lead dioxide (PbO_2) in acidic bromide solution. *Environ. Sci. Technol.* **2010**, *44* (10), 3895−3900.

(22) Zhang, Y.; Lin, Y. P. Determination of PbO_2 formation kinetics from the chlorination of Pb(II) carbonate solids via direct PbO_2 measurement. *Environ. Sci. Technol.* **2011**, *45* (6), 2338−2344.

(23) Pleskov, Y. V.; Filinovskii, V. Y. *The Rotating Disc Electrode*; Consultants Bureau: New York, 1976; p 297.

(24) Frisch, M. J.; Trucks, G. W.; Schlegel, H. B.; Scuseria, G. E.; Robb, M. A.; Cheeseman, J. R.; Scalmani, G.; Barone, V.; Mennucci, B.; Petersson, G. A.; Nakatsuji, H.; Caricato, M.; Li, X.; Hratchian, H. P.; Izmaylov, A. F.; Bloino, J.; Zheng, G.; Sonnenberg, J. L.; Hada, M.; Ehara, M.; Toyota, K.; Fukuda, R.; Hasegawa, J.; Ishida, M.; Nakajima, T.; Honda, Y.; Kitao, O.; Nakai, H.; Vreven, T.; Montgomery, J. A., Jr.; Peralta, J. E.; Ogliaro, F.; Bearpark, M.; Heyd, J. J.; Brothers, E.; Kudin, K. N.; Staroverov, V. N.; Kobayashi, R.; Normand, J.; Raghavachari, K.; Rendell, A.; Burant, J. C.; Iyengar, S. S.; Tomasi, J.; Cossi, M.; Rega, N.; Millam, J. M.; Klene, M.; Knox, J. E.; Cross, J. B.; Bakken, V.; Adamo, C.; Jaramillo, J.; Gomperts, R.; Stratmann, R. E.; Yazyev, O.; Austin, A. J.; Cammi, R.; Pomelli, C.; Ochterski, J. W.; Martin, R. L.; Morokuma, K.; Zakrzewski, V. G.; Voth, G. A.; Salvador, P.; Dannenberg, J. J.; Dapprich, S.; Daniels, A. D.; Farkas, O.; Foresman, J. B.; Ortiz, J. V.; Cioslowski, J.; Fox, D. J. *Gaussian 09*, Revision A.01; Gaussian, Inc.: Wallingford, CT, 2009.

(25) Chai, J.-D.; Head-Gordon, M. Systematic optimization of long-range corrected hybrid density functionals. *J. Chem. Phys.* **2008**, *128* (8), 084106.

(26) Dunning, T. H. Jr. Gaussian basis sets for use in correlated molecular calculations. I. The atoms boron through neon and hydrogen. *J. Chem. Phys.* **1989**, *90* (2), 1007−1023.

(27) Kendall, R. A.; Dunning, T. H. Jr.; Harrison, R. J. Electron affinities of the first-row atoms revisited. Systematic basis sets and wave functions. *J. Chem. Phys.* **1992**, *96* (9), 6796−6806.

(28) Peterson, K. A.; Figgen, D.; Goll, E.; Stoll, H.; Dolg, M. Systematically convergent basis sets with relativistic pseudopotentials. II. Small-core pseudopotentials and correlation consistent basis sets for the post-d group 16−18 elements. *J. Chem. Phys.* **2003**, *119* (21), 11113−11123.

(29) Scalmani, G.; Frisch, M. I. Continuous surface charge polarizable continuum models of solvation. I. General formalism. *J. Chem. Phys.* **2010**, *132* (11), 114110.

(30) ChemCraft, Tool for Treatment of Chemical Data. http://www.chemcraftprog.com.Accessed in July, 2011.

(31) Ai, S.; Wang, Q.; Li, H.; Jin, L. Study on production of free hydroxyl radical and its reaction with salicylic acid at lead dioxide electrode. *J. Electroanal. Chem.* **2005**, *578* (2), 223−229.

(32) Kim, J.; Korshin, G. V. Examination of in situ generation of hydroxyl radicals and ozone in a flow-through electrochemical reactor. *Ozone Sci. Eng.* **2008**, *30* (2), 113−119.

(33) Elovitz, M. S.; von Gunten, U. Hydroxyl radical/ozone ratios during ozonation processes. I. The Rct concept. *Ozone Sci. Eng.* **1999**, *21* (3), 239−260.

(34) Kao, N. H.; Su, M. C. Statistical study of instantaneous demand of *para*-chlorobenzoic acid as an ozone/hydroxyl radical probe compound. *Environ. Eng. Sci.* **2009**, *26* (4), 791−798.
(35) Wander, M. C. F.; Clark, A. E. Hydration properties of aqueous Pb(II) ion. *Inorg. Chem.* **2008**, *47* (18), 8233−8241.
(36) McQuinn, K.; Hof, F.; McMcIndoe, J. S.; Chen, X.; Wu, G.; Stace, A. J. Evidence of asymmetric cation salvation from the instability of $[Pb(H_2O)_n]^{2+}$ complexes. *Chem. Commun.* **2009**, *27*, 4088−4090.
(37) Persson, I.; Lyczko, K.; Lundberg, D.; Eriksson, L.; Płaczek, A. Coordination chemistry study of hydrated and solvated lead(II) ions in solution and solid state. *Inorg. Chem.* **2011**, *50* (3), 1058−72.
(38) Yu, X. Y. Critical evaluation of rate constants and equilibrium constants of hydrogen peroxide photolysis in acidic aqueous solutions containing chloride ions. *J. Phys. Chem. Ref. Data* **2004**, *33* (3), 747−763.
(39) Yu, X. Y.; Barker, J. R. Hydrogen peroxide photolysis in acidic aqueous solutions containing chloride ions. I. chemical mechanism. *J. Phys. Chem. A* **2003**, *107* (9), 1313−1324.
(40) Grebel, J. E.; Pignatello, J.; Mitch, W. A. Effect of halide ions and carbonates on organic contaminant degradation by hydroxyl radical-based advanced oxidation processes in saline waters. *Environ. Sci. Technol.* **2010**, *44* (17), 6822−6828.